Layer-by-Layer Polyelectrolyte/Inhibitor Nanostructures for Metal Corrosion Protection

Daria V. Andreeva,[†] Ekaterina V. Skorb,*,[‡] and Dmitry G. Shchukin[‡]

Physical Chemistry II, University of Bayreuth, Universitätstrasse 30, Bayreuth 95440, Germany, and Max Planck Institute of Colloids and Interfaces, Wissenschaftspark Golm, Am Mühlenberg 1, Golm 14476, Germany

ABSTRACT Multicomponent coating formed by polyelectrolyte multilayers opens new opportunities for anticorrosion protection. Here we demonstrate a novel method of corrosion protection based on formation and deposition of polyelectrolyte multilayers on aluminum and steel alloys, analysis of different polyelectrolyte compositions (strong−strong, strong−weak, weak−weak) as candidates for corrosion protective layers. The multilayer nanonetwork exhibits very high corrosion protection because of the nature and versatility of the polyelectrolyte complex. The anticorrosion activity of the coating is based on the following mechanisms: (1) pH buffer formed by polybase and polyacid complex suppress pH changes caused by corrosion degradation; (2) coating regeneration and defect elimination due to relative mobility of polymer chains in swollen state; (3) polyelectrolyte layers form a carrier for inhibitor allowing its release on demand; (4) polyelectrolyte nanonetwork provides a barrier between surface and environment. We optimize the coating preparation conditions in a rational way by applying various polyacid−polybase combinations. We use the scanning vibration electrode technique to characterize corrosion protection of the novel coating.

KEYWORDS: layer-by-layer • polyelectrolyte • multilayers • corrosion • coating

1. INTRODUCTION

The extremely high economic and environmental impact of corrosion of metallic structures raised large scientific interest to this problem and requires an interdisciplinary approach. Mostly protective coatings are applied to metallic surfaces to create a passive barrier between metal and aggressive environment. Development of a new generation of anticorrosion coatings possessing both passive matrix functionality and active response to changes in the local environment has raised high interest in material science during the past few years. For example, since Mengoli et al. (1) was the first to examine the protective behavior of polyaniline on stainless steel and then in 1985, DeBerry (2) showed that the electrochemically synthesized polyaniline acts as corrosion protective layer on stainless steel, the number of papers that use conductive polymers as protective corrosion layer increases every year (3). Simultaneously for the time being, active corrosion protection aims to recover the substrate from corrosion degradation restoring material properties (functionality) if the passive coating matrix is broken and if corrosion of the substrate has started. Furthermore, smart coatings have to control the release of the active and repairing material within a short time following the beginning of the corrosion process. This leads to attaining a triggering mechanism for the coating matrix.

The multicomponent nanonetwork formed by polyelectrolyte multilayers using the Layer-by-Layer (LbL) technique (4−8) could offer new opportunities for anticorrosion coatings. The LbL deposition procedure involves the stepwise electrostatic assembly of oppositely charged species (e.g., polyelectrolytes and inhibitors or others: proteins, nanoparticles) on the substrate surface with nanometer scale precision and allows the formation of a coating with multiple functionality. The coating properties can be controlled by the number of deposition cycles and the types of polyelectrolytes used (9−11). Polyelectrolytes exhibit very good adhesion to the substrate surface and are able to seal surface defects (12). The conformation of polyelectrolytes is mostly dependent on their nature and adsorption conditions and much less dependent on the substrate and charge density of the substrate surface (13). Polyelectrolyte coatings are expected to cover many kinds of surfaces including nonionic and a polar substrates (14). The polyelectrolyte multilayers offer a broad range of applications in the fields of nonlinear optics, light emission, sensing, separation, bioadhesion, biocatalytic activity, drug delivery, and specific bioapplications based on surface modifications (4−14).

In recent years, polyelectrolyte multilayers have attracted great interest in corrosion protection (12). Corrosion processes are accompanied by a number of reactions changing the composition and properties of both metal surface and local neighboring environment (e.g., formation of oxides, diffusion of metal cations into the coating matrix, local changes of pH and electrochemical potential) (15, 16). An approach to prevent corrosion propagation on metal surfaces is the suppression of accompanying physicochemical reactions. Polyelectrolytes are macromolecules carrying a relatively large number of functional groups that either are charged or can become charged under suitable conditions (17). Polyelectrolyte films are able to change their chemical composition with pH because the degree of dissociation of
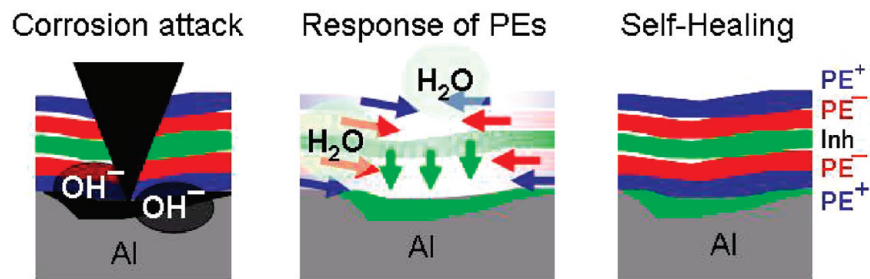
FIGURE 1. Schematic mechanism of self-healing action of a "smart" polyelectrolyte anticorrosion coating. Corrosion attack causes pH change of the system stimulating response of the polyelectrolyte coating: pH buffering, rearrangement of polymer chains and release of corrosion inhibitor. (PE$^+$, positively charged polyelectrolyte; PE$^-$, negatively charged polyelectrolyte; Inh, corrosion inhibitor).

the polyelectrolytes is influenced by the local pH value. The films can be enriched in one polymer compared to the other by fabrication in a pH regime where one of the polymers is weakly charged while the other is strongly charged. Active species deposited as a component of the polyelectrolyte nanonetwork or as a dopant can be released on demand. The sensitivity of the polyelecrolyte film to a variety of physical and chemical conditions (like pH-shift or mechanical impact) of the surrounding media provides the ability of regulated release of the inhibitor species entrapped into multilayers. The schematic mechanism of a smart self-healing process is shown in Figure 1.

In our previous publications (18, 19), we proposed the following mechanisms of the response of the polyelectrolyte multilayer system to corrosion attack: (i) the polyelectrolytes have pH-buffering activity and can stabilize the pH (between 5 and 7.5) at the metal surface in corrosive media; (ii) the inhibitors are released from polyelectrolyte multilayers only after start of the corrosion process and directly in the rusted area, preventing corrosion propagation; (iii) polyelectrolytes forming the coating are relatively mobile and have the tendency to seal and to eliminate the mechanical cracks of the coating. Thus, the polyelectrolyte nanonetwork is effective in both suppression of corrosion propagation and healing of first traces of corrosion microdefects.

Here, we focus on anticorrosion behavior of three main types of polyelectrolyte nanonetworks differed in their pH buffering activity, degree of swelling, and therefore, coating mobility and barrier properties. Combination of strong–weak, weak–weak, and strong–strong polyelectrolytes are chosen to reveal a contribution of each corrosion–protection mechanism of polyelectrolytes: pH buffering, regeneration, and barrier to aggressive species. Several issues related to formation of the coating and their anticorrosion activities are addressed. The first issue is the nature of the alloy surface, polymer adhesion to the surface, and coating stability in an aggressive environment. Aggressive solutions as well as temperature changes or UV irradiation could alter the structural integrity of multilayer films. The second issue is related to the anticorrosion activity of the coating. The sensitivity of the nanonetwork formed by different polyelectrolytes to external stimuli generated by corrosion degradation (pH changes, interruption of coating integrity) is most important and studied. We used IR spectroscopy to analyze chemical composition of the surface coating and interlayer interactions, atomic force microscopy, and scanning electron

microscopy to investigate the morphology for different preparations and treatment and the scanning vibration electrode technique to quantify space- and time-dependent corrosion protection to contribute a mechanistic understanding. Simultaneously, we boarded the spectrum of metals that could be protected by applying Lbl polyelectrolyte/inhibitor nanonetwork.

2. EXPERIMENTAL SECTION

2.1. Metal Plate Surface Pretreatment. Metal samples were degreased in isopropanol flow and rinsed in purified water. Before polymer deposition the surface of the metal plates was etched by ultrasound (Ultrasonic Processor CV 33 Sonics Inc. (Switzerland) operating at 20 kHz with maximal output power of 500 W) within 10 min. The detailed studied between the influence of sonochemicaly etching onto metal plate morphology could be found in ref 20.

2.2. Deposition of the Polyelectrolyte Coating. The poly-(ethyleneimine) (PEI, branched MW∼600−1000 kDa, Sigma-Aldrich), poly(styrene sulfanate) sodium salt (PSS, MW∼70 kDa, Sigma-Aldrich), poly(acrylic acid) sodium salt (PAA, 5 kD, Sigma-Aldrich), poly(diallyldimethylammonium chloride) (PDADMAC, 200−350 kD, 20 wt % in water, Sigma-Aldrich) layers were deposited on degreased and etched metal by spray drying, spin coating and dip coating from 2 mg/mL^{-1} solution of polyelectrolytes in a water/ethanol (1:1, v/v) mixture. After each deposition step, the samples were washed in a water/ethanol mixture and dried with a nitrogen stream. 8-Hydroxyquinoline (8-HQ, Sigma-Aldrich) was deposited by the same method as a cationic polyelectrolyte between two PSS layers from 10 wt % solution of 8-HQ in ethanol.

2.3. Infrared Reflection Absorption Spectroscopy (IRRA). Spectra were acquired with an IFS 66 FT-IR spectrometer from Bruker (Ettlingen, Germany). The infrared beam is directed through the external port of the spectrometer and is subsequently reflected by three mirrors in a rigid mount before being focused on the sample surface. A KRS-5 wire grid polarizer is placed into the optical path directly before the beam hits the sample surface. The reflected light is collected at the same angle as the angle of incidence. The light then follows an equivalent mirror path and is directed onto a narrow band mercury−cadmium−telluride detector, which is cooled by liquid nitrogen. The entire experimental setup is enclosed to reduce relative humidity fluctuations. For all measurements at 40 mN/m, p-polarized radiation was used at an angle of incidence of 70°. A total of 128 scans were acquired with a scanner velocity of 20 kHz at a resolution of 8 cm^{-1}.

2.4. Microscopy Studies. Scanning electron microscopy (SEM) measurements were conducted with a Gemini Leo 1550 instrument at an operation voltage of 3 keV. Samples were sputtered with gold. Atomic force microscopy (AFM) measurements were performed in air at room temperature using a
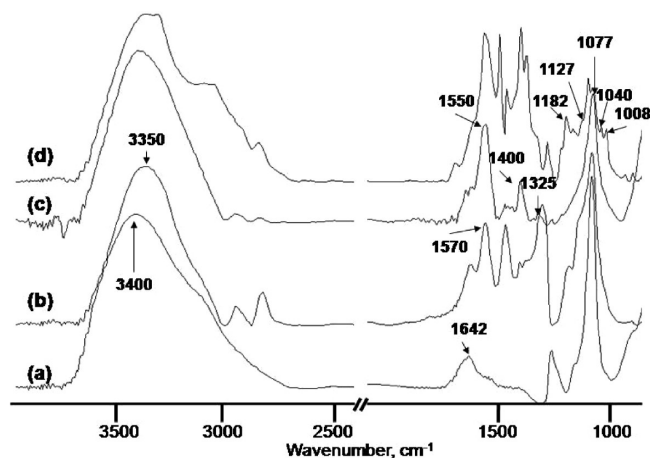
FIGURE 2. IRRA spectra of the surface of (a) the pretreated aluminum alloy, (b) the aluminum alloy covered by a PEI monolayer, (c) PEI−PAA, and (d) one PEI−PSS bilayer.

Nanoscope III multimode AFM (Digital Instruments Inc., USA) operating in tapping mode.

2.5. Scanning Vibrating Electrode Technique (SVET). The SVET experiments were performed by using the equipment supplied by Applicable Electronics (Forestdale, MA) (16). Samples were prepared for SVET measurement by cutting into 1×2 cm^2 plates; 2×2 mm^2 areas were opened for the measurements, and other parts of the samples were protected masking with a Polyester 5 adhesive tape (3M Company). The anticorrosion coating of each sample was scratched to introduce a defect extending to the metal surface; the area of the defect ranges from 0.1 to 0.3 mm^2. The sample was mounted in a homemade epoxy−resin cell. The immersion solution was 0.1 M NaCl solution in the case of aluminum and steel and 0.5 M H$_2$SO$_4$ in the case of nickel. Scans were initiated within 5 min of immersion and were collected every 2 h for the duration of the experiment, typically 20 h. Each scan consisted of 400 data points obtained on a 20×20 grid, with an integration time of 1 s per point. A complete scan required 10 min. The normal or z component of the measured current density in the plane of the vibrating electrode is plotted in 3D format over the scan area, with positive and negative current densities representing anodic and cathodic regions, respectively. To observe the degradation of the aluminum plates, we formed 2 mm long scratches in the coatings. The samples were then introduced into the SVET device and 0.1 M NaCl solution was added immediately before the first scan. As a reference, aluminum plates covered by standard sol−gel films were used. The synthesis and deposition of sol−gel were described in ref 21.

3. RESULTS AND DISCUSSION
3.1. Coating Composition and Structure.
3.1.1. Surface Pretreatment and Modification. The polyelectrolyte multilayers are formed by alternating adsorption of positively and negatively charged polyelectrolytes. The design of the polyelectrolyte anticorrosion system is schematically shown in Figure 1. Positively charged poly-(ethyleneimine) (PEI) and poly(diallyldimethylammonium) chloride (PDADMAC) and negatively charged poly(styrene sulfonate) (PSS) and poly(acrylic acid), nanolayers are deposited on the pretreated (19) metal alloy. The IRRA spectrum of freshly activated aluminum plates is shown in Figure 2a. It is characterized by absorption bands near 3400, 3100, 1642, 1400, and 1077 cm^{-1}, and from these bands the oxide was identified as pseudoboehmite (22). The dominating

band at 1077 cm^{-1} is attributed to vibrations of A1-OH. The OH stretching absorption bands can be seen at 3400 cm^{-1} with shoulders at 3100 and 3570 cm^{-1} (23). The bending mode of adsorbed H$_2$O is seen at 1642 cm^{-1} (24). The peak width depends on the heterogeneity of the molecular environment of hydrogen-bonded water molecules. In general, the more disordered the molecular environment, the broader the band. Besides the red shift in the OH stretching frequencies, formation of hydrogen bonds between water molecules is also accompanied by an increase in the integrated cross-section. However, the band at 1642 cm^{-1} is relatively narrow for randomly distributed hydrogen-bonded water molecules, and therefore, could demonstrate formation of an ordered oxide layer on the surface of the aluminum alloy.

3.1.2. Layers Formed by Weak−Strong and Weak−Weak Polyelectrolytes. The infrared spectrum of the PEI film (Figure 2b) is characterized by bands at 3500 and 3300 cm^{-1} (−N−H stretch of primary and secondary amines); 2930 and 2840 cm^{-1} (−C−H stretch); 1590 cm^{-1} (−N−H bending of primary amine); 1455, 1350, and 1290 cm^{-1} (−C−H bending); 1150−900 cm^{-1} (broad absorption due to −C−N stretch) (25). In the spectrum of PEI adsorbed on the aluminum surface all peaks from NH groups and some from −C−H bending are slightly shifted to the low frequency part of the spectrum. The −N−H stretch of the primary and secondary amines is observed at 3350 cm^{-1} with a shoulder at 3250 cm^{-1}, the −N−H bending of primary amine is detected at 1570 cm^{-1}. The decrease in the frequencies of the valence vibrations of the N−H bond in the complexes indicates an increase in its polarity, and consequently, an increase in the acidic properties of the protons.

In the PSS spectrum (Figure 2d), the bands at 1127 and 1192 cm^{-1} are associated with the sulfonate anion, −SO$_3^-$, and are sensitive to interactions of the sulfonate with its environment (26). The shift of the band at 1192− 1182 cm^{-1} is one piece of the evidence of complex formation between PSS and PEI. The symmetric −SO$_3^-$ stretching vibration observed in the region of 1040 cm^{-1} and the band at 1008 cm^{-1} assigned to the in-plane bending vibrations of the para-substituted benzene ring, with the sulfonate group being the substitute group, are characteristic for PSS. Finally, a broad band between 3200 and 3600 cm^{-1} and H$_2$O scissor vibration between 1700 and 1570 cm^{-1} can also be observed due to the presence of water (27). Peaks at 1130 and 1011 cm^{-1} can be assigned to the in-plane skeleton vibration of the benzene ring and the in-plane bending vibration of the benzene ring.

If PAA is used as a negative coating component instead of PSS the most pronounced changes in the frequencies (Figure 2c) are the appearance of two new bands at 1550 and 1400 cm^{-1} (28). These bands can be assigned to the asymmetric and symmetric stretching vibrations of carboxylic anions, COO$^-$. The characteristic carbonyl group frequency at 1710 cm^{-1} is not observed in the spectrum of the PEI−PAA coating, clearly demonstrating the complex formation between COO$^-$ and NH$^+$ groups.
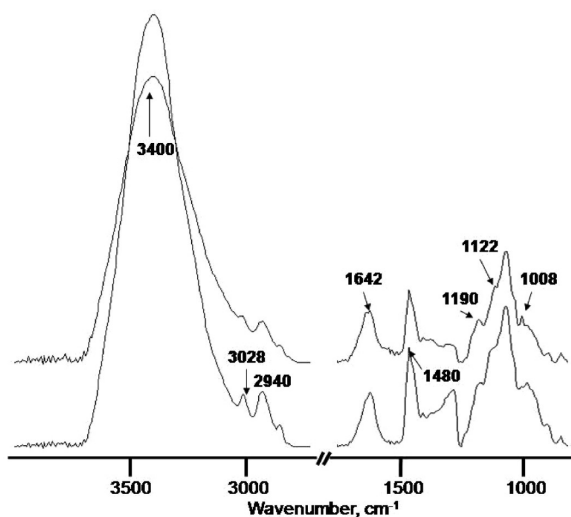
FIGURE 3. IRRA spectra of the surface of the pretreated aluminum alloy covered by (a) a PDADMAC monolayer and (b) one PDADMAC—PSS bilayer.

FIGURE 4. IRRA spectra of the surface of the PEI—PSS coating (10 bilayers) prepared by (a) spray-coating, (b) spin-coating, and (c) dip coating.

All spectra of the polyelectrolyte nanolayers exhibit a decrease of the intensity of the peaks from the surface of the aluminum alloy. Most sensitive to the layer formation is the band at 1642 cm^{-1} ascribed to adsorbed water. After deposition of the first polyelectrolyte layer this band disappears. Therefore, polyelectrolytes effectively adhere to the surface of aluminum. The low-frequency shifts of the characteristic bands prove the interaction between PEI and the aluminum surface and the formation of the polyelectrolyte complexes.

The thickness of ten polyelectrolyte bilayers is estimated by AFM and ellipsometry to about 80 nm for PEI—PSS and 800 nm for PEI—PAA. The calculated thickness of one PEI—PSS bilayer is about 8 nm and of one PEI—PAA bilayer about 80 nm. Therefore, the used coating preparation condition leads to bulk adsorption of PAA and formation of thick PAA layers.

It should be also noted the influence of pH on layer build-up of weak polyelectrolytes, the amount of polymer adsorbed can be manipulated to suit the desired thickness of the multilayer film. However, Al plates covered by Al oxide are sensitive to pH changes and Cl ions; therefore, we could not apply very high and low pH. In our case, pH was adjusted to 5.5 for PAA and 9 for PEI in order to achieve the maximal thickness of the multilayers at pH values harmless for the Al substrate covered by Al oxide, which is sensitive to high and low pH (29).

3.1.3. Layers Formed by Strong—Strong PEs.
The infrared spectrum (Figure 3a) for a PDADMAC layer exhibits its most intense bands at 3400, 3028, 2940, and 1480 cm^{-1} (30). Adsorption of PSS adds bands at 1190, 1122, and 1008 cm^{-1} (Figure 3b). The problem with spectrum interpretation in the case of the PDADMAC-PSS complex is caused by the low adhesion of PDADMAC to the surface, and therefore, formation of a very thin and discontinuous layer of PSS. This also explains that the peak from the adsorbed water at 1642 cm^{-1} can be clearly observed in the spectra of the PDADMAC—PSS covered samples.
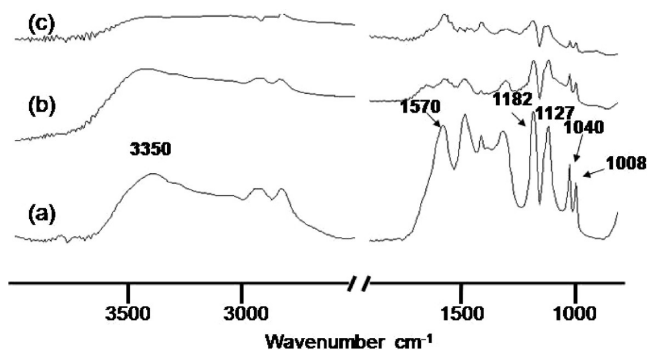
Therefore, the polyelectrolyte nanolayers do not significantly replace water on the aluminum surface. However, after that, a continuous layer deposition is reached with a thickness of the final 10 bilayer coating of 200 nm as measured by AFM.

3.1.4. Coating Preparation.
Three convenient methods can be used for the polyelectrolyte coating preparation: spray-drying, spin-coating, and dip-coating. All of these methods can be adjusted to the used system. We compare the PEI—PSS coating prepared by all of these methods by using IRRA spectroscopy. The spectra of the films formed by spray-drying (Figure 4a), spin-coating (Figure 4b) and dip-coating (Figure 4c) exhibit significantly different peak intensity. The spectra obviously show that spray drying allows preparing the thickest polyelectrolyte films. The bands from PEI and PSS are much more pronounced in the spectrum of the sample prepared by spray drying. The characteristic bands of the aluminum surface at 1077 and at 1400 cm^{-1} as well as a peak of the water adsorbed on the aluminum surface at 1642 cm^{-1} disappear in all three spectra. Therefore, all preparation methods result in successful modification of the surface by the polyelectrolytes.

3.1.5. Morphology of the Coatings.
AFM and SEM images (Figure 5) confirm the homogeneous deposition of all multilayer combinations on the surface of the aluminum alloy. All PE complexes cover the substrate sealing the surface defects. Both PEI—PAA (Figure 5a) and PEI—PSS (Figure 5b) form a continuous nanonetwork slightly differing in the surface roughness. Because of formation of a very thin layer (80 nm) the PEI—PSS coating repeats the initial surface topology of the aluminum and exhibits a rougher surface compared to the 800-nm-thick PEI—PAA coating. The SEM images of both coatings (Figure 5a,b, bottom images) demonstrate a tendency in formation of homogeneous coatings with increase of the number of polyelectrolyte multilayers. Even the deposition of only two (PEI—PSS)$_2$ bilayers leads to the formation of a protective film maintaining the surface morphology of the initial aluminum alloy and resulting in a very thin functional layer. The increase in the number of deposited layers up to 10 decreases the surface roughness, filling the pores on the aluminum surface with polyelectrolytes. These 10 bilayers form a dense, homogeneous, and defect-free protective coating that provides both buffering
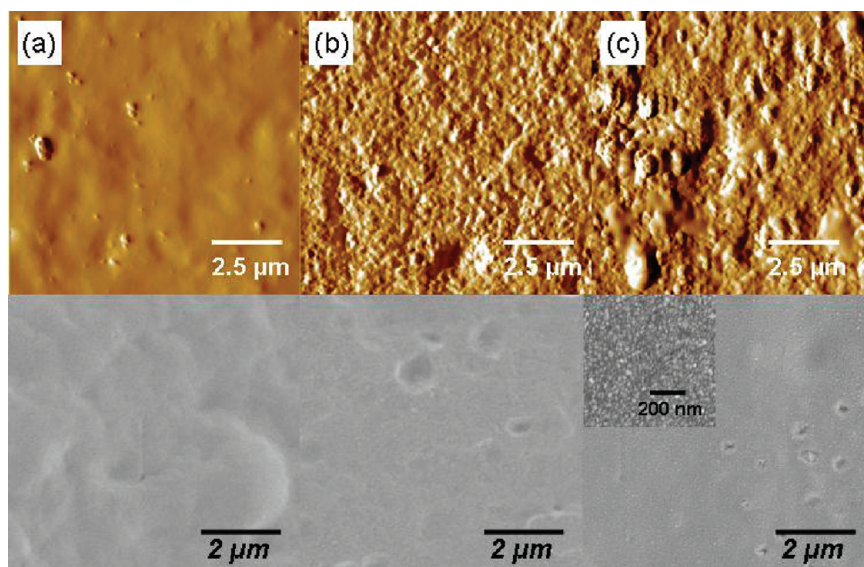
FIGURE 5. AFM (above) and SEM (below) images of the aluminum surface covered by (a) (PEI−PAA)$_{10}$, (b) (PEI−PSS)$_{10}$, and (c) (PDADMAC−PSS)$_{10}$.
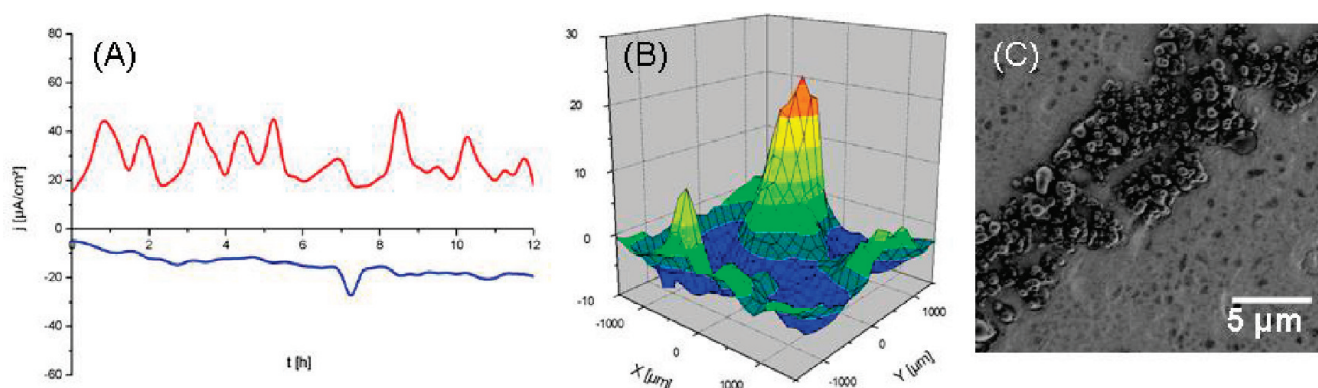

FIGURE 6. (A) Time dependence of the corrosion propagation of the scratched aluminum alloy covered by the (PDADMAC−PSS)$_{10}$ coating obtained by scanning vibrating electrode technique: red curve, anodic current; blue curve, cathodic current (scale units, μA cm^{-2}; spatial resolution, 150 μm; solution, 0.1 M NaCl); (B) current density map of the sample after 3 h of immersion in 0.1 M NaCl; (C) scanning electron microscopy image of the scratch covered by corrosion products.

ability inherent to polyelectrolyte multilayers and barrier protection properties (see below).

In contrast, the PDADMAC−PSS coating (Figure 5c) consists of approximately 20−40 nm aggregates homogeneously distributed on the surface. Formation of the aggregates could be caused by poor adhesion of the PDADMAC on the aluminum surface due to weak affinity of this polyelectrolyte to the aluminum surface. These results are in good agreement with the spectroscopic analysis and confirm the formation of a stable and continuous coating by PEI−PSS and PEI−PAA pairs and agglomerates of PDADMAC−PSS.

3.2. Mechanism of Anticorrosion Protection of Polyelectrolyte Coating. *3.2.1. Buffering Activity of the Polyelectrolyte Multilayers.* The approach to prevention of corrosion propagation on metal surfaces achieving the self-healing effect is based on suppression of accompanying physicochemical reactions. The corrosion processes are followed by changes of the pH value in the corrosive area and metal degradation (31−34). Local pH neutralization could be achieved by the formation of the coating with pronounced pH-buffering activity on the metal

surface which could stabilize the pH between 5 and 7.5 values at the metal surface in corrosive media. We investigated the anticorrosion activity of three polyelectrolyte systems: weak polycation, PEI, and weak polyanion, PAA; PEI and strong polyanion, PSS; two strong polyelectrolytes, PDADMAC and PSS, by the scanning vibrating electrode technique (SVET). The SVET method delivers current density maps over a selected surface of the sample, thus allowing the monitoring of local cathodic and anodic activity in the corrosion zones.

Figure 6A demonstrates the time monitoring of the anodic (red line) and cathodic (blue line) activity on the aluminum surface covered by a PDADMAC - PSS nanonetwork in 0.1 M NaCl solution for 12 h. To provoke corrosion degradation of the surface the polyelectrolyte coating was scratched before immersion in NaCl solution. Figure 6B shows the current density map of the sample after 3 h of immersion. Both anodic (orange peak) and cathodic peaks (blue gaps) appear with experiment time resulting in defect propagation throughout the whole surface of the sample. The corroded scratch can be seen in the SEM images (Figure 6C).
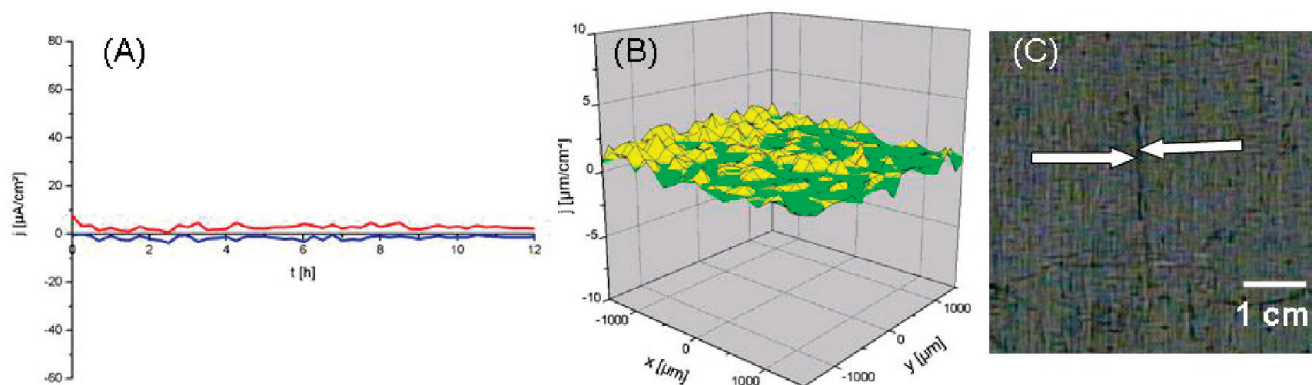
FIGURE 7. (A) Time dependence of the current density changes of the scratched aluminum alloy covered by the (PEI−PSS)$_{10}$ coating obtained by scanning vibrating electrode technique: red curve, anodic current; blue curve, cathodic current (scale units, μA cm^{-2}; spatial resolution, 150 μm; solution, 0.1 M NaCl); (B) snapshot measured in 3 h of the experiment time; (C) photograph of the behavior of the scratched surface during the SVET experiments. The scratch is highlighted by the arrows.

Both strong polyelectrolytes carry high charge densities over wide pH ranges. Therefore, interaction between them is too strong to be altered by pH change. Furthermore, because of the formation of the strong complex between PDADMAC and PSS, the interaction of PDADMAC with the substrate is very weak.

Weak polyelectrolytes are increasingly used in multilayer thin films because greater control over film properties can be achieved by varying the ionization of the weakly charged groups through pH adjustments. Therefore, we expect a different current density map for the substrates coated with multilayers composed of a combination of weak and strong PEs (Figure 7). PEI−PSS coating exhibits very high anticorrosion protection. The scratched aluminum surface is shown in Figure 7C. The scratch without any traces of corrosion degradation is highlighted by the arrows. No ionic flux can be seen on the time monitoring measured by using SVET during 12 h. The control snapshot (Figure 7B) exhibits only background noise.

As well as the PEI−PSS nanonetwork, the film of two weak polyelectrolytes PEI and PAA is able to protect the aluminum surface in aggressive media. Comparing the SVET results obtained for PEI−PSS with those for the samples covered by PEI−PAA coating, the beginning of the corrosion process is observed at 7 h immersion time (Figure 8A, left). The PEI−PAA buffering system suppresses propagation of corrosion degradation within the next 30 min (Figure 8A, right). Time monitoring (Figure 8B) proves suppression of corrosion within the experimental time of 12 h. A significant corrosion activity is observed only once during the experiment. The weakness in corrosion resistance of the PEI−PAA multilayers in the comparison with PEI-PSS multilayers might be explained by a higher degree of swelling of this polyelectrolyte's increasing of the permeability of the coating.

The differences between strong and weak polyelectrolyte pairs are presumed to reflect the relative degree of association of oppositely charged polyelectrolyte segments. Polymer pairs that form stronger complexes are expected to better associate in contact with aqueous solutions and would thus be less sensitive to pH changes in contrast to weak−strong and weak−weak polyelectrolyte pairs.

3.2.2. Self-Curing Due to Mobility of the Polyelectrolyte System.
pH changes following the corrosion process cause ionization of the functional groups of the weak polyelectrolytes, which results in an increased repulsion between uncompensated charges. Small counterions can penetrate the layer structure to compensate these charges. The higher ionic concentration inside polyelectrolyte multilayers as compared to the surrounding solution increases the osmotic pressure, resulting in permeation of water into the polyelectrolyte multilayers. Thus, the polyelectrolyte multilayers start to swell, and therefore increase their mobility. Figure 9 shows SEM images of the PEI−PAA-covered aluminum plates after 12 h immersion in 0.1 M NaCl. The scratched surface tends to recover in aqueous solution due to chain rearrangement in the swollen polymer multilayers. It is seen in Figure 9b that corrosion peak measured by SVET could disappear because of mobility of the polyelectrolyte system.

3.2.3. Polyelectrolyte Multilayers As a Carrier for Corrosion Inhibitors.
A corrosion inhibitor incorporated into the protective coating as a component of the LBL film is responsible for the most effective mechanism of corrosion suppression. Quinolines are environmentally friendly corrosion inhibitors attracting more and more attention as an alternative to the harmful chromates. The inhibiting activity of the quinolines was studied for copper and aluminum corrosion. 8-HQ was found to prevent the adsorption of chloride ions, thus improving the corrosion resistance because of the formation of an insoluble chelate of aluminum which protects the metal substrate (35−37). Both mechanical (mechanical scratch) and chemical (due to changes of local pH) rupture of the polyelectrolyte network cause the release of the encapsulated inhibitor in the damaged part of the metal surface only. Therefore, the inhibitor release occurs in response to corrosion attack resulting in termination of the corrosion process and prolongation of corrosion protection.

Incorporation of 8HQ into PEI−PSS polyelectrolyte multilayers between PSS layers was confirmed by IRRA. Bands absorbed at 1606, 1506, 1498, and 1475 cm^{-1} (not shown)
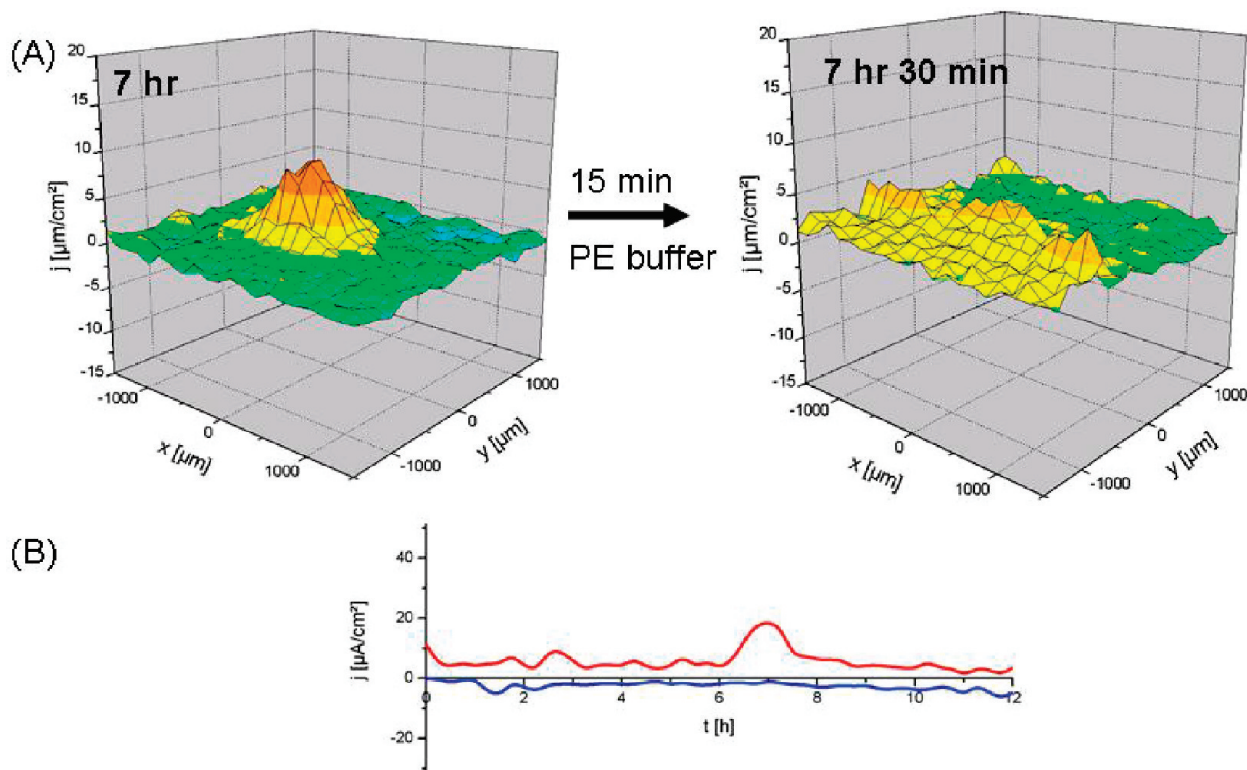
FIGURE 8. (A) Scanning vibrating electrode measurements of the ionic currents above the surface of the scratched aluminum alloy covered by the (PEI−PAA)$_{10}$ coating (scale units, μA cm^{-2}; spatial resolution, 150 μm; solution, 0.1 M NaCl). Experiment time is 7 h (left); experiment time is 7 h 30 min (right). (B) Time dependence of the current density changes of the scratched aluminum alloy covered by the (PEI−PAA)$_{10}$ coating: red curve, anodic current; blue curve, cathodic current.
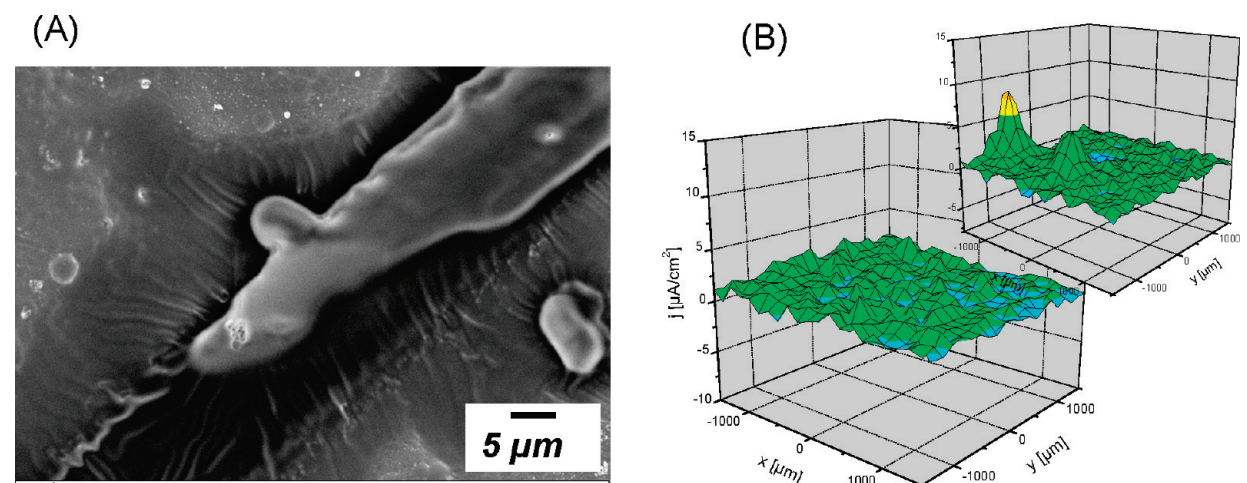

FIGURE 9. (A) Scanning electron microscopy image of the surface of the PEI−PAA coating after 12 h immersion in 0.1 M NaCl; (B) scanning vibrating electrode measurements of the ionic currents above the surface in 12 h (inset, in 10 h 30 min).

can be assigned to ring vibrations and the one at 1373 cm^{-1} to C−H bending of the >CHO group in the 8HQ (38). In the solid state, the infrared absorption spectrum of 8HQ shows a broad band due to OH stretching vibrations in the range 3100−3200 cm^{-1}, which is characteristic of hydrogen bonding between the OH groups and the nitrogen atoms.

In the SVET experiment of the aluminum alloy coated by polymer/inhibitor film after immersion in 0.1 M NaCl solution the coating was also mechanically damaged. Neither anodic activity nor corrosion products were observed over an experiment time of 16 h. Corrosion damage of the

scratched surface of the aluminum covered by PEI−PSS multilayers loaded with 8-HQ after 24 h immersion in 0.1 M NaCl was studied by SEM. The corrosion degradation of the ZrO$_x$/SiO$_x$ sol−gel-coated sample can be clearly observed in Figure 10. The substrate covered by PEI−PSS−8−HQ coating exhibits a small area of corrosion damage. Though the corrosion process was initiated by the aggressive NaCl solution in both cases, the corrosion is localized and suppressed better by the protective polyelectrolyte coating containing the inhibitor in the multilayer structure than by the ZrO$_x$/SiO$_x$ sol−gel film.
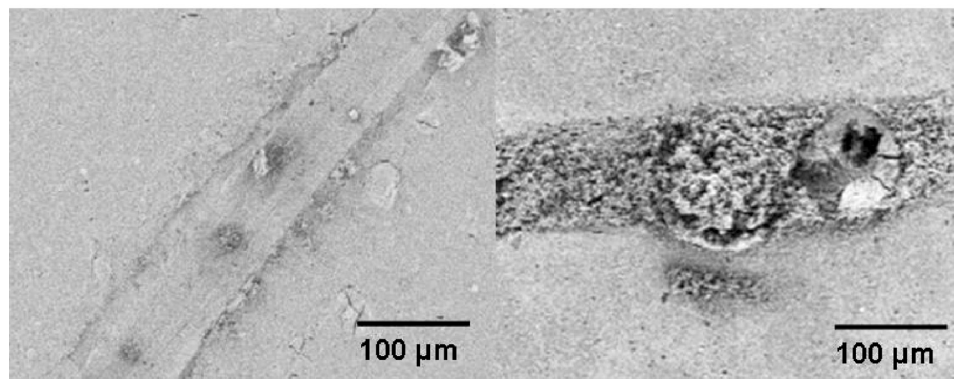
FIGURE 10. Scanning electron microscopy images of (A) the scratched area of the polyelectrolyte/inhibitor coating and (B) standard sol−gel coating after 24 h immersion in 0.1 M NaCl.
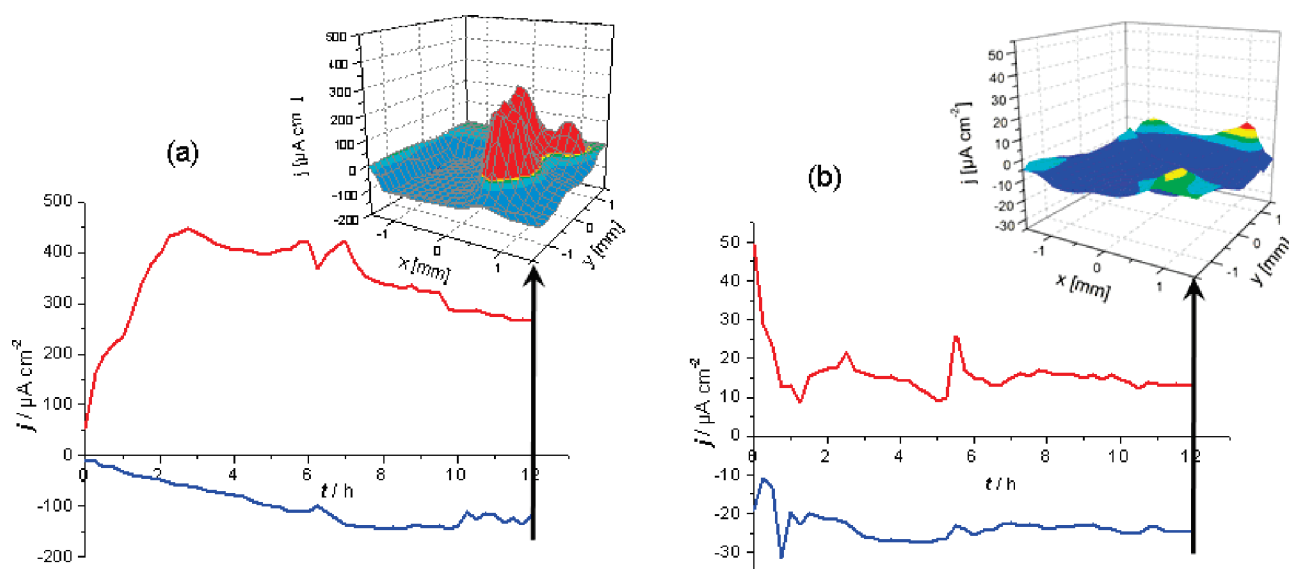

FIGURE 11. Scanning vibrating electrode measurements (SVET) of kinetics of maximum and minimal ionic currents activity above the surface of (a) uncovered steel and (b) steel covered with "smart" polyelectrolyte anticorrosion coating. Insets show the 3D ionic current maps in 12 h after corrosion test start. Note differing scales.

3.2.3.1. Polyelectrolyte/Inhibitor Sandwichlike Nanostructures for Steel Corrosion Protection.

On the basis of the previously suggested mechanism of anticorrosion response of the polyelectrolyte multilayer system, it was expected that polyelectrolyte/inhibitor sandwichlike nanostructures could be effectively used for steel corrosion protection. Indeed, the SVET corrosion study show very nice protective prospects. The bare heat treating carbon steel exhibited several regions of anodic activity, reflecting sites of localized corrosion in Figure 11a.

Onto the bare steel, the corrosion has the tendency to increase, which is well- seen from maximum and minimum of corrosion activity measured in time. In contrast, the coating with preformed polyelectrolyte/inhibitor sandwich like multilayers in their composition shows a well-pronounced self-healing effect. It is seen in Figure 11b that the corrosion peak has a tendency to disappear during the corrosion process. Simultaneously, the corrosion level is totally different in time; in the case of uncoated surface the level of corrosion is much higher. The novel protective method also shows promising results for copper and nickel corrosion protection.

CONCLUSIONS

A polyelectrolyte nanonetwork has been shown to offer many potential advantages for corrosion-inhibiting coatings. The main mechanism of anticorrosion protection is based on the pH buffering activity of complexes formed by weak−strong and two weak polyelectrolytes. The polyelectrolyte nanonetwork can be successfully loaded with corrosion inhibitors providing controlled release on demand. The corrosion inhibitor inserted into multilayer structure lends the system a great versatility of being tuned to specific demands concerning substrate and pH. The other properties of the polyelectrolytes−the relative mobility and passive barrier properties−have a slight effect on the coating efficiency. Here, we presented a novel multifunctional polyelectrolyte nanonetwork that is able to respond to physical and chemical changes caused by corrosion degradation.

REFERENCES AND NOTES

(1) Mengoli, G.; Munari, M. T.; Bianco, P.; Musiani, M. M. *J. Appl. Polym. Sci.* **1981**, *26*, 4247–4257.

(2) Deberry, D. W. *J. Electrochem. Soc.* **1985**, *132*, 1022–1026.

(3) Li, X. G.; Huang, M. R.; Zeng, J. F.; Zhu, M. F. *Colloids Surf., A* **2004**, *248*, 111–120.

(4) Decher, G. *Science* **1997**, *277*, 1232–1237.

(5) Stuart, M. A. C.; Huck, W. T. S.; Genzer, J.; Muller, M.; Ober, C.; Stamm, M.; Sukhorukov, G. B.; Szleifer, I.; Tsukruk, V. V.; Urban, M.; Winnik, F.; Zauscher, S.; Luzinov, I.; Minko, S. *Nat. Mater.* **2009**, *9*, 101–113.

(6) Klitzing, R. v. In *Colloid Stability and Application in Pharmacy Colloids and Interfaces Science*; Tadros, T., Ed.; Wiley-VCH, Weinheim, Germany, 2007; Vol. 3.

(7) Bucur, C. D.; Sui, Z.; Schlenoff, J. B. *J. Am. Chem. Soc.* **2006**, *128*, 13690–13691.

(8) Agarwal, M.; Lvov, Y.; Varahramyan, K. *Nanotechnology* **2006**, *9*, 5319–5325.

(9) DeLongchamp, D. M.; Kastantin, M.; Hammond, P. T. *Chem. Mater.* **2003**, *15*, 1575–1586.

(10) Shiratori, S. S.; Rubner, M. F. *Macromolecules* **2000**, *33*, 4213–4219.

(11) Voigt, A.; Donath, E.; Moehwald, H. *Macromol. Mater. Eng.* **2000**, *282*, 13–16.

(12) Farhat, T. R.; Schlenoff, J. B. *Langmuir* **2001**, *17*, 1184–1192.

(13) Tjipto, E.; Quinn, J. F.; Caruso, F. *J. Polym. Sci., Part A: Polym. Chem.* **2007**, *45*, 4341–4351.

(14) Vagharchakian, L.; Desbat, B.; Henon, S. *Macromolecules* **2004**, *37*, 8715–8720.

(15) Roberge, P. R. *Corrosion Basics*, 2nd ed.; NACE Press: Houston, TX, 2005; p 364.

(16) Frankel, G. S.; Landolt, D. In *Encyclopedia of Electrochemistry*; Stratmann, M., Bard, A. J., Eds.; Wiley-VCH: Weinheim, Germany, 2003; Vol. 4, Chapter 1.

(17) Nalwa, H. S.; *Handbook of Polyelectrolytes and Their Applications*; American Scientific: Valencia, CA, 2002.

(18) Andreeva, D. V.; Fix, D.; Moehwald, H.; Shchukin, D. G. *Adv. Mater.* **2008**, *20*, 2789–2794.

(19) Andreeva, D. V.; Fix, D.; Moehwald, H.; Shchukin, D. G. *J. Mater. Chem.* **2008**, *18*, 1738–1740.

(20) Skorb, E. V.; Shchukin, D. G.; Möhwald, H.; Andreeva, D. V. *Nanoscale* **2010**, *2*, 722–727.

(21) Skorb, E. V.; Fix, D.; Andreeva, D. V.; Shchukin, D. G.; Möhwald, H. *Adv. Funct. Mater.* **2009**, *19*, 2373–2379.

(22) Boerio, F. J.; Gosselin, C. A.; Dillingham, R. G.; Liu, H. W. *J. Adhes.* **1981**, *13*, 159–179.

(23) Wolska, E.; Szajda, W. *J. Appl. Spectrosc.* **1983**, *38*, 137–140.

(24) Al-Abadleh, H. A.; Grassian, V. H. *Langmuir* **2003**, *19*, 341–347.

(25) Haas, H. C.; Schuler, N. W.; Macdonald, N. R. *J. Polym. Sci.* **1972**, *10*, 3143–3158.

(26) Tran, Y.; Auroy, P. *J. Am. Chem. Soc.* **2001**, *123*, 3644–3654.

(27) Yang, J. C.; Jablonsky, M. J.; Mays, J. W. *Polymer* **2002**, *43*, 5125–5132.

(28) Moharram, M. A.; Balloomal, S.; El-Gendy, H. M. *J. Appl. Polym. Sci.* **1996**, *59*, 987–990.

(29) Shiratori, S. S.; Rubner, M. F. *Macromolecules* **2000**, *33*, 4213–4219.

(30) Gregoriou, V. G.; Hapanowicz, R.; Clark, S. L.; Hammond, P. T. *Appl. Spectrosc.* **1997**, *51*, 470–476.

(31) Zhang, W. L.; Frankel, G. S. *J. Electrochem. Soc.* **2002**, *149*, 510.

(32) Schmutz, P.; Frankel, G. S. *J. Electrochem. Soc.* **1998**, *145*, 2285–2295.

(33) Zhang, W. L.; Frankel, G. S. *Electrochim. Acta* **2002**, *48*, 1193.

(34) Frankel, G. S. *J. Electrochem. Soc.* **1998**, *145*, 2186–2198.

(35) Garriguess, L.; Pebere, N.; Dabosi, F. *Electrochim. Acta* **1996**, *41*, 1209–1215.

(36) Cicileo, G. P.; Rosales, B. M.; Farela, F. E.; Vilche, J. R. *Corros. Sci.* **1998**, *40*, 1915–1926.

(37) Szunerits, S.; Walt, D. R. *Anal. Chem.* **2002**, *74*, 886–894.

(38) Halls, M. D.; Arosa, R. *Can. J. Chem.* **1998**, *76*, 1730–1736.